Published in final edited form as:
Biochemistry. 2009 December 1; 48(47): 11243–11251. doi:10.1021/bi901501a.

IDENTIFICATION OF THE RATE-DETERMINING STEP OF tRNA-GUANINE TRANSGLYCOSYLASE FROM *E. coli*†

George A. Garcia*, **Stephanie M. Chervin**, and **Jeffrey D. Kittendorf**
Department of Medicinal Chemistry, College of Pharmacy, University of Michigan, Ann Arbor, MI 48109-1065

Abstract

The modified RNA base queuine (7-(4,5-*cis*-dihydroxy-1-cyclopenten-3-ylaminomethyl)-7-deazaguanine) occurs in tRNA via a unique base exchange process catalyzed by tRNA-guanine transglycosylase (TGT). Previous studies have suggested the intermediacy of a covalent TGT-RNA complex. To exist on the reaction pathway, this covalent complex must be both chemically and kinetically competent. Chemical competence has been demonstrated by the crystal structure studies of Xie *et al.* (*Nature Structural Biology* (2003) 10, 781–788); however, evidence of kinetic competence had not yet been established. The studies reported here unequivocally demonstrate that the TGT-RNA covalent complex is kinetically capable of occurring on the TGT reaction pathway. These studies further suggest that product RNA dissociation from the enzyme is overall rate-limiting in the steady-state. Interestingly, studies comparing RNA with a 2′-deoxyriboside at the site of modification suggest a role for the 2′-hydroxyl group in stabilizing the growing negative charge on the nucleophilic aspartate (264) as the glycosidic bond to the aspartate is broken during covalent complex breakdown.

Over one hundred chemically distinct modified bases are known to occur in RNA, the majority of which occur in tRNA (1). Of these, queuine (Q) stands out for several reasons. Structurally, queuine is the only modified base that is not a purine or pyrimidine analog. Instead, queuine features a pyrrolo-pyrimidine heterocyclic scaffold that is further elaborated through exocyclic chemical modifications. Perhaps most interestingly, the mechanism of incorporation of queuine into tRNA is unique. The queuine base is post-transcriptionally introduced into tRNA via a transglycosylation reaction that is catalyzed by tRNA-guanine transglycosylase (TGT) (Figure 1). Among the known modified bases, only pseudouridine is installed in an analogous manner whereby pseudouridine synthase breaks and reforms the glycosidic bond to the uracil (2).

As with pseudouridine synthase, the chemical mechanism of the TGT reaction has been studied for some time. Two distinct mechanisms have been proposed and subsequently investigated for the TGT catalyzed base-exchange reaction. It was first envisaged that a dissociative mechanism, involving the intermediacy of an oxocarbonium ion, could drive the cleavage of

†This work was supported in part by the National Institutes of Health (GM065489, GAG; GM07767, JDK trainee), and the University of Michigan, College of Pharmacy, Vahlteich and UpJohn Research Funds.

Address correspondence to: George A. Garcia, PhD, Department of Medicinal Chemistry, College of Pharmacy, University of Michigan, Ann Arbor, Michigan 48109-1065. Phone: (734) 764-2202; Fax: (734) 647-8430; gagarcia@umich.edu.

SUPPORTING INFORMATION AVAILABLE

The following supporting information is available: MALDI-TOF mass spectrometry analyses of hairpin RNAs, table of two-state fit parameters, TGT active site sequence alignments showing conservation of aspartates, example of a thermodynamic fit of SPR association peak values for three lanes of a single sensor chip, and an example of a complete set of fitted sensorgrams for a single lane (i.e., one trial for a single RNA). This material is available free of charge via the internet at http://pubs.acs.org.

the glycosidic bond leading to the incorporation of the modified base. Alternatively, and equally plausible, the TGT reaction may proceed through a covalent TGT-RNA intermediate (3) in an associative mechanism similar to that of retaining glycosyl hydrolases (4) (Figure 2A). In fact, biochemical studies from our laboratory have implicated the associative mechanism and the involvement of two active site aspartate residues in the reaction (5,6). Consistent with the associative mechanism, we have previously shown that the *E. coli* TGT follows ping-pong kinetics (7), with RNA binding first, followed by guanine release, binding of $preQ_1$, and finally release of product RNA (Figure 2B). More recently, the X-ray crystal structure of a TGT-RNA complex (Figure 3) has revealed that aspartate 264 can form a covalent bond with the ribose of the RNA. Furthermore, upon addition of $preQ_1$, the covalent complex converted to free TGT and product RNA.

While compelling, these studies are not sufficient to definitively prove the intermediacy of the covalent complex. For example, it is possible that during the crystallization process, aspartate 264 could have trapped a carbonium ion intermediate. To be considered an intermediate in an enzymic reaction, the covalent complex must be both chemically competent (i.e., it must form from substrates and react to form the correct products) and kinetically competent (i.e., the intermediate must form and breakdown at a rate equal to or greater than k_{cat}). In order to provide clear evidence for the associative mechanism, we have carried out studies to determine the kinetic competence of the covalent complex. The results of these experiments indicate that the TGT-RNA covalent complex is kinetically competent and therefore can exist on the TGT reaction pathway. Through this analysis, we have also identified the rate-limiting step in the TGT reaction and find evidence suggesting a role for the 2′-hydroxyl group of the ribose in the TGT reaction.

EXPERIMENTAL PROCEDURES

Reagents

Unless otherwise specified, reagents were purchased from Sigma or Aldrich. Isopropyl β-D-thiogalacto-pyranoside (IPTG) and dithiothreitol (DTT) were from Invitrogen. Ampicillin, kanamycin and chloramphenicol were from Boehringer Mannheim. HEPES (1 M solution, pH 7.3), precast PhastGels and SDS buffer strips were from Pharmacia. Tris•HCl buffer was from Research Organics. His•Bind® resin was from Novagen. Bactotryptone and yeast extract were from Difco. Bradford reagent and BSA standards were from Bio-Rad. [8-^{14}C] Guanine (56 mCi/mmol) was from Moravek. Reagents for RNA chemical synthesis were from Applied Biosystems, with the exception of the RNA and DNA (dG) phosphoramidite monomers and the CPG columns, which were from Glen Research. *E. coli* tRNA-guanine transglycosylase (TGT) and the D264N mutant were prepared as previously described (5,6).

Chemical Synthesis of RNA Mini-helices

The hairpin RNAs ECYMH (5′-GGGAGCAGACUGUAAAUCUGCUCCC-3′) and $(dG)_{34}$ECYMH (5′-GGGAGCAGACUdGUAAAUCUGCUCCC-3′) were synthesized by automated chemical synthesis performed on an Expedite nucleic acid synthesis system (model 8909, PerSeptive Biosystems) and purified as previously described (5,6) or were purchased from Dharmacon. Biotinylated hairpin RNAs (bio-ECYMH and bio-$(dG)_{34}$ECYMH) were purchased from Dharmacon.

Preparation of $PreQ_1$-containing RNA Mini-helices

In a reaction volume of 200 μL, the substrate RNA (ECYMH, $(dG)_{34}$ECYMH, bio-ECYMH, or bio-$(dG)_{34}$ECYMH, 80 μM) was incubated with $preQ_1$ (200 μM) and TGT (1.4 μM) in bicine reaction buffer (bicine, 50 mM pH 8.1) at 37 °C for 18 h. The reaction was quenched by precipitation upon the addition of 10 M ammonium acetate (low sodium) to a final

concentration of 1 M and 750 μL of ethanol (reagent grade) and cooled at −20 °C for 8 h. The precipitated RNA was recovered by centrifugation and purified twice more by ethanol precipitation. The resulting RNA pellet was resuspended in ultrapure water to a final concentration of 50 μM and stored at −20 °C. The guanine/preQ$_1$ substitution was confirmed by MALDI mass spectrometry by confirming the 28 mass unit differential between the guanine-containing and preQ$_1$-substituted RNA (see Supplementary Material).

Steady-state Kinetics for ECYMH and (dG)$_{34}$ECYMH

Substrate RNA at concentrations ranging from 0.1 to 30.0 μM was incubated with [^{3}H] preQ$_1$ (20 μM) in bicine assay buffer (bicine (50 mM pH = 8.1), $MgCl_2$ (20mM), DTT (5 mM)) at 37 °C. The reaction was initiated by the addition of *E. coli* TGT to a final enzyme concentration of 100 nM. At specific intervals (1, 4, 8, 12, 20 min) an aliquot (70 μL) of the reaction was quenched with 10 μL of NaOAc (3 M, pH 5.5) followed immediately by precipitation in 900 μL ethanol. The quenched samples were cooled to −20 °C for 2 h. The precipitated RNA substrate was captured by filtration through a Whatman GF/C membrane. The membrane was immersed in BioSafeII LSC cocktail and the amount of tritium incorporation was determined by liquid scintillation counting. Initial velocities (v_i) were determined from plots of pmol [^{3}H] preQ$_1$ incorporated versus time. k_{cat} and K_M values were determined from nonlinear fits of v_i versus RNA substrate concentration to equation 1 (Michaelis-Menten).

$$v_i = \frac{(k_{cat}[TGT][RNA])}{(K_M + [RNA])} \quad (1)$$

Rate of Covalent Intermediate Formation

The apparent rate of formation of the TGT-RNA covalent intermediates for ECYMH and (dG)$_{34}$ECYMH were assayed as previously described (8) with modifications. A KinTek RQF-3 rapid chemical quench-flow apparatus was charged with drive buffer (bicine (50 mM, pH 8.1)) and SDS quench buffer (tris•HCl (60 mM, pH 7.0), 2% SDS) and equilibrated to 37 °C. The sample port A was loaded with a solution of enzyme, TGT (15 μM), in bicine assay buffer and sample port B was loaded with a solution of RNA substrate (30 μM) also in bicine assay buffer. Aliquots (15 μL) of each reagent were incubated in the mixing chamber for various periods (0.5 –120.0 s) and quenched automatically with SDS buffer (90 μL). The mixtures were incubated for an additional hour at room temperature prior to SDS-PAGE band-shift analysis. Aliquots (4 μL) of each reaction were loaded onto a gradient 8–25% polyacrylamide gel (Pharmacia Phast System, now GE Healthcare) and run under denaturing conditions following the vendor protocols. The gel was removed from the plastic backing and stained with Sypro-Red. The bands were visualized by green laser excitation (532 nm) and fluorescent detection using a Typhoon 9200 gel imaging system (Molecular Dynamics). The percent covalent intermediate was calculated from the band volumes, which were quantified with the ImageQuant software package (Molecular Dynamics) as described (8). Assays were conducted in triplicate, and the apparent first-order rate constants ($k_{formation}$) for formation of the TGT-RNA intermediates were determined by exponential fits of the data to equation 2:

$$y = M\left(1 - e^{(-k_{formation} * t)}\right) \quad (2)$$

where y is % covalent complex formed, *t* is time in seconds and *M* is the maximum % covalent complex.

Isolation of The TGT-$(dG)_{34}$ECYMH covalent intermediate

TGT (50μM) and $(dG)_{34}$ECYMH (75 μM) were incubated in bicine assay buffer in a total reaction volume of 100 μL for 20 min at 37 °C. The reaction was cooled to 4 °C and diluted with 200 OL of Ni^{+2} column binding buffer (tris•HCl (20 mM, pH 7.9), NaCl (500 mM), imidazole (10 mM)). The covalent intermediate and any unreacted free TGT were isolated from the reaction mixture via Ni^{+2} affinity chromatography, taking advantage of the his-tagged TGT. Ni-NTA resin (50 OL, His•Bind®, Novagen) was added to the mixture, and the slurry was applied to a disposable plastic column. The column was washed with 20 mM imidazole in binding buffer to remove unbound RNA. The TGT-$(dG)_{34}$ECYMH intermediate and free TGT were eluted with 250 mM imidazole in binding buffer. The eluted material was exchanged into bicine buffer and analyzed by SDS-PAGE. The isolation of the covalent intermediate was confirmed by MALDI-TOF mass spectrometric analysis as described above. The matrix was 2,4,6-trihydroxyacetophenone (10 mg/mL) and ammonium citrate (5 mg/mL) in acetonitrile/water 1:1. The following ions were detected: (m+1)/1 = (52449) and (m+1)/2 = (26187).

Rate of Covalent Intermediate Breakdown

The apparent rate of formation of the TGT-$(dG)_{34}$ECYMH intermediate was assayed in a fashion similar to that for the apparent rate of formation of the covalent intermediate. The TGT-$(dG)_{34}$ECYMH and TGT mixture (15 μL, 6 μM) was mixed with a solution of $preQ_1$ (15 μL, 1.2 mM) and quenched in SDS buffer over a time course ranging from 0.01 to > 20 sec using a KinTek rapid-quench apparatus as described above. The quenched samples were then separated by SDS-PAGE and quantified as described above. Assays were conducted in triplicate and the apparent first-order rate constant ($k_{breakdown}$) for breakdown of the TGT-$(dG)_{34}$ECYMH intermediate was determined by exponential fit of the data to equation 3:

$$y=(M_1 - M_2)\left(e^{(-k_{breakdown}t)}\right)+M_2 \quad (3)$$

where y is % covalent complex remaining, t is time in seconds, M_1 is the maximum % covalent complex and M_2 is minimum % covalent complex.

Association and Dissociation Kinetics via Surface Plasmon Resonance

Surface plasmon resonance studies were carried out on a BIAcore 3000 (GE Healthcare Life Sciences). Strepavidin (SA) sensor chips were purchased from GE Healthcare. Running buffer was the same bicine assay buffer used for the steady-state kinetics with the addition of 0.1 % Tween (which had no effect on enzyme activity, data not shown). The sensor chip surface was equilibrated with running buffer at 10 μL/min for 2–4 hours. Biotinylated RNA (e.g., bio-$(dG)_{34}$ECYMH) was loaded onto the sensor chip via sequential injections of 5 or 10 μL. Lane 1 of the sensor chip was used as a blank control lane. The biotinylated RNA injections were repeated, as needed, to obtain approximate loading of 800, 1500 and 2500 response units (RUs) in lanes 2, 3 & 4, respectively. The RNAs were stably associated with the sensor chip surface as evidenced by constant RU values for each lane after replicate regeneration injections and throughout the course of each experiment.

Ten different concentrations of TGT (D264N), ranging from 0.05 μM to 7.5 μM, were flowed over the sensor chip at a rate of 10 μL/min and a temperature of 37 °C. Injection volumes varied between 20 and 40 μL in order to establish equilibrium binding during the association phase. The dissociation phase was monitored for 120–240 seconds. Regeneration of the sensor chip (e.g., complete dissociation of TGT (D264N)) was achieved by injecting 20–40 μL of 2 or 6 M guanidine hydrochloride in running buffer.

Sensorgram data were analyzed using the BIA evaluation software (GE Healthcare Life Sciences). The data best fit to the "two-state (conformational change) model (equation 4):

$$\mathbf{A}+\mathbf{B}\underset{k_{off}}{\overset{k_{on}}{\rightleftharpoons}}\mathbf{AB}\underset{k_{reverse}}{\overset{k_{forward}}{\rightleftharpoons}}\mathbf{AB}^{*} \tag{4}$$

The equilibrium binding responses (association phase peaks) were fit via non-linear regression to equation 5 using Kaliedagraph:

$$RRU=\frac{(k_{assn}[TGT][RNA])}{(K_D*+[RNA])} \tag{5}$$

where RRU is the relative response units and K_D* is the "thermodynamic" dissociation constant.

RESULTS

Steady-state Kinetics for ECYMH and $(dG)_{34}$ECYMH

In previous studies, we observed that hairpin RNAs (ca. 25 bases in length) corresponding to the anticodon stem-loop of TGT-substrate tRNAs are suitable substrates for the *E. coli* TGT (9–11). We have also shown that within these substrates, the guanosine corresponding to the tRNA position 34 can be replaced with a 2′-deoxyriboside without affecting steady-state kinetic values (11). The relative ease of synthesis and biotinylation of hairpin RNAs prompted their use in studying the kinetic details of the TGT reaction. The biotinylation of the substrate RNAs was necessary for the surface plasmon resonance experiments. Importantly, control experiments demonstrated that this chemical modification had no effect on the interaction of the RNA with TGT (data not shown). Steady-state kinetic parameters were determined for ECYMH and $(dG)_{34}$ECYMH by following the incorporation of [^{3}H] $preQ_1$ into the RNA substrate (Figure 4). The values were essentially identical with a slightly higher k_{cat} for $(dG)_{34}$ECYMH.

Rate of Covalent Intermediate Formation

We have reported using rapid-quench kinetics as a technique to characterize covalent enzyme-RNA intermediates (8). The apparent rates of formation of the covalent intermediates for ECYMH and $(dG)_{34}$ECYMH were determined with this technique (Figure 5, Table 1). Again, the apparent rates of formation for both RNAs are essentially identical. In this experiment, guanine is released, either bound to the covalent enzyme-RNA complex or free in solution. Given that TGT can catalyze a guanine for guanine base-exchange reaction, it is possible that the displaced guanine can attack the covalent complex reforming non-covalently-bound substrate RNA. This activity accounts for the equilibrium of covalent and non-covalent complexes that is observed in these experiments. Interestingly, the two RNAs achieve different equilibrium extents of covalent intermediate formation (Figure 5B), with ECYMH reaching ca. 25% and $(dG)_{34}$ECYMH at ca. 55%.

Rate of Covalent Intermediate Breakdown

The rate of covalent intermediate breakdown proved to be much more difficult to study. To do so, the TGT-RNA covalent intermediate must first be formed and isolated. Once isolated, the breakdown of the intermediate can be evaluated using the same rapid-quench strategy employed in the formation studies. Unfortunately, only the $(dG)_{34}$ECYMH-TGT covalent intermediate proved amenable to isolation, and even so, the isolated species consisted of a 1:1

mixture of unbound enzyme and covalent intermediate (Figure 6A). Analysis of the rapid quench data suggests that the breakdown of this intermediate follows biphasic kinetics (Figure 6B). Interestingly, the first phase of the reaction was too rapid to obtain accurate data. Consequently, the first data point was omitted in the fitting of the second, slower phase. Due to the technical difficulties associated with these experiments, the apparent rate of breakdown for $(dG)_{34}$ECYMH (Table 2) should be viewed as an estimate only for the slower phase.

Association and Dissociation Kinetics

Surface Plasmon Resonance (SPR) was employed to determine the rates of association and dissociation of the RNA and TGT. Wild-type TGT will rapidly form a covalent complex with RNA bound to the sensor chip, complicating association and dissociation studies. Therefore, we elected to use a TGT mutant, TGT(D264N), which we have previously shown to be inactive and incapable of forming the covalent intermediate, while maintaining the ability to bind non-covalently to RNA (5,6). The biotinylated RNAs were bound to a streptavidin-coated sensor chip and TGT(D264N) was flowed over the chip. Supplementary Figure 2 shows an example of a sensorgram for one concentration of TGT(D264N) flowing over three RNA-bound lanes (different RNA loadings indicated) and one control lane on a single chip.

For each concentration of TGT(D264N), the association phase was followed to the point where equilibrium binding was established (e.g., the association peak). The average relative response unit values corresponding to the association peaks for the various TGT(D264N) concentrations were fit to determine "thermodynamic" K_D^*s for the RNAs (Figure 7, Table 2). Different amounts of RNA were intentionally loaded in the three sample lanes on each sensorchip to control for loading-dependent artifacts (see Discussion). One would expect that the maximum amount of TGT(D264N) bound in each lane (e.g., RRU plateau values) would correlate with the amount of RNA loaded. This is in fact the case within each chip, as shown in Supplementary Figure 3 (an example of the thermodynamic fits for each lane of a single chip). The trend in plateau values matches the trend in RNA loading for the lanes. This was observed for all RNAs examined in these studies (data not shown). Interestingly, from chip to chip (i.e., different RNAs), the plateau RRU values do not correlate with the average RNA loadings. Thus, it is likely that the absolute RRU values vary more from chip to chip than with the loading.

The association and dissociation phases were globally fit to a two-state ("conformational change") model (eq. 4). (Supplementary Figure 4 shows one example of the fitted association and dissociation curves.) The fit yielded values for the rate constants shown in Equation 4. (Supplementary Table 2 shows all of these values.) In Table 2, the values for k_{on}, k_{off} and K_D calculated from these rate constants are reported. Fitting to a two-state model is not sufficient to prove the existence of a conformational change, as SPR is insensitive to conformational change (BIA Evaluation Software Manual). To date, independent evidence is lacking to support a conformational change in the TGT reaction. Furthermore, due to technical reasons discussed above, an inactive TGT mutant is employed in these SPR studies. It is possible that this mutant enzyme or the RNA substrate may exhibit a conformational change that would not be present in the wild-type TGT reaction where the binding of the heterocyclic substrate would drive the reaction forward. Given these issues, the conformational change is somewhat underdefined, therefore we choose to define K_D as the equilibrium constant for the initial binding of RNA and exclude the putative subsequent conformational change. As shown in Table 2, the K_Ds calculated from the association and dissociation rate constants match very well with the thermodynamic K_D^*s determined from the association peak fits, consistent with the above discussion.

DISCUSSION

Previously published data from our laboratory strongly supports an associative molecular mechanism for the TGT reaction (5,7). The X-ray crystal structure of the TGT from *Z. mobilis*, solved in the presence of the RNA substrate, offers further evidence for this hypothesis (Figure 3) (12). Specifically, this structure unequivocally demonstrates that TGT is capable of forming a covalent linkage with RNA. Together, these biochemical and structural studies implicate the formation of a covalent intermediate during TGT catalysis.

However, proof of the existence of an intermediate on a reaction pathway requires three generally accepted criteria (13). First, the intermediate should be isolable. Second, the reaction intermediate should be chemically competent (i.e., forms from substrates and can turn over to the correct products). Finally, the reaction intermediate should be kinetically competent (i.e., can form and react at a rate that is $\geq k_{cat}$). The elucidation of the TGT-RNA co-crystal structure has indeed demonstrated that a TGT-RNA covalent intermediate is isolable. Furthermore, upon soaking the crystals with $preQ_1$, Xie *et al.* observed turnover of the TGT-RNA intermediate which generated free enzyme (12). This observation is in strong agreement with work from our laboratory in which it was observed that the TGT-RNA covalent complex could be converted to free TGT in solution upon the addition of $preQ_1$. Together, these independent observations indicate that the TGT-RNA covalent intermediate is chemically competent.

Previously, Geeganage and Frey (14) employed a rapid-quench approach to determine the kinetic competence of a uridyl-enzyme intermediate in the galactose-1-phosphate uridylyltransferase reaction in which the formation of the uridyl-enzyme intermediate was followed upon mixing a single concentration of enzyme with saturating substrate under single turnover conditions (see Fig 3 in their paper). Comparison of the resulting first-order rate constant (281 s^{-1}) with k_{cat} (62 s^{-1}) led to the authors' conclusion that the formation of the covalent intermediate is kinetically competent. To establish the kinetic competence of the putative TGT-RNA covalent intermediate, we carried out a similar study in an effort to determine the apparent first-order rate constant of intermediate formation for wild-type TGT. In the case of the TGT reaction, this observed rate constant ($k_{formation}$) is a combination of at least four individual rate constants, as shown in Figure 2, and that additional information is required in order to de-convolute $k_{formation}$ to obtain the microscopic rate constant for the chemical step of intermediate formation. The observed formation rate constants for ECYMH and $(dG)_{34}$ECYMH are essentially identical (ca. 0.12 s^{-1}, Table 1) and ten-fold faster than k_{cat} (0.01 s^{-1}) (Table 2), thereby demonstrating that formation of the covalent intermediate is fast enough to be on the TGT reaction pathway. Moreover, given that k_{cat} is representative of the rate-limiting step, this comparison indicates that formation of the covalent intermediate is not rate-limiting in the TGT reaction.

The breakdown of the TGT-RNA covalent complex was also interrogated using the same rapid-quench approach. Unfortunately, the TGT-ECYMH covalent complex could not be isolated in sufficient quantities for characterization. However, the covalent complex with $(dG)_{34}$ECYMH was amenable to isolation and follow up study. The breakdown of this covalent complex exhibited biphasic breakdown kinetics (Figure 6). The slower phase was determined to be 0.50 s^{-1}, which, like the rate of formation ($k_{formation}$), is much faster than k_{cat}. These studies where carried out under pseudo-first order conditions (e.g., saturating $preQ_1$), eliminating the $preQ_1$ binding step in the kinetics. Therefore this observed breakdown rate can be viewed as a lower limit for the true chemical breakdown step as any back reaction, reforming the covalent intermediate prior to product release, would reduce the observed rate. This proves that even the slower phase of covalent complex breakdown is also fast enough to be on the TGT reaction pathway and is not the rate-limiting step for the reaction. It should be noted that this experimental procedure involves denaturation of the enzyme-RNA complex; therefore the loss

of covalently bound complex is being monitored, regardless of whether the RNA is still non-covalently bound (i.e., RNA dissociation is not a factor).

The results from this work demonstrate that the covalent TGT-RNA complex is kinetically capable of existing on the TGT reaction pathway (i.e, kinetically competent). Moreover, because the rate constants measured in these studies are both faster than k_{cat}, neither chemical step (formation nor breakdown) nor binding of substrate RNA (part of the apparent rate of formation) can be rate-limiting in the TGT reaction. Thus, the identity of the rate-limiting step was still unknown.

Surface plasmon resonance, whereby biotinylated RNAs were bound to streptavidin-coated sensor chips, was employed to identify the rate-limiting step in the TGT reaction. It was immediately apparent that wild-type TGT could not be utilized in these experiments due to its propensity to bind the RNA and quickly form the covalent complex. This would preclude our ability to study the dissociation of the TGT-RNA non-covalent complex. To overcome this issue, an inactive TGT mutant (TGT(D264N)) in which the nucleophilic aspartate (264) is mutated to asparagine, was employed in our SPR experiments. It has previously been demonstrated that this TGT mutant binds substrate RNA but is catalytically inactive and cannot form the covalent intermediate (6). Using this mutant, the association and dissociation rate constants, as well as the corresponding equilibrium dissociation constants for substrate (ECYMH and $(dG)_{34}$ECYMH) and product (($preQ_1)_{34}$ECYMH and ($dpreQ_1)_{34}$ECYMH) RNAs were determined (Table 2 and Supplementary information). The experiments were conducted with three different loading levels of RNA on each chip relative to a control lane that contained no RNA. Similar kinetic values were obtained for all three RNA loading levels, eliminating the possibility of any “rebinding” or other loading-dependent artifacts in the SPR experiments. Within each chip, the maximum RRU values for each lane correlated with the RNA loading (Supplementary Figure 3), as would be expected. “Thermodynamic” fits of the association phase peak values versus the enzyme concentration yielded K_D values that correlated well with those from the kinetic fits (Table 2). These controls establish the validity of the SPR kinetic determinations.

The resulting sensorgrams were globally fit using the BIA Evalution software package. The association rate constants were all very high (Table 2). For example, at saturation (e.g., 20 OM RNA) the association rate for ECYMH would be ~0.8 s^{-1}, roughly 80-fold faster than k_{cat}. This fast association rate is consistent with the apparent rate of formation (~0.1 s^{-1}) that was measured in the rapid-quench studies, suggesting that the observed rate of formation can be attributed to the chemical step. In contrast the dissociation rate constants (Table 2) are much slower and comparable to k_{cat} (e.g., ($preQ_1$)ECYMH dissociation rate 0.010 s^{-1}, k_{cat} 0.0094 s^{-1}). As mentioned above, the kinetically determined K_D values correlate very well with those from the thermodynamic fits (Table 2).

Figure 8 shows the kinetic mechanism for TGT with the rate constants that have been determined in these studies. Lower limits for the dissociation of guanine (> 0.01 s^{-1}) and the association of $preQ_1$ (> 10^4 M^{-1} s^{-1}) can be set given that they cannot be lower than k_{cat}. (i.e, @ ~10^{-6} M $preQ_1$ (~K_M) one would observe an on rate of 0.01 s^{-1}). By assuming that the K_M values for both guanine and $preQ_1$ approximate K_D values and are in the micromolar range, lower limits for the association of guanine (> 10^4 M^{-1} s^{-1}, same estimation as for $preQ_1$) and the dissociation of $preQ_1$ (> 0.01 s^{-1}) can be set by simple division ($K_D = k_{off}/k_{on}$). Our SPR experiments indicate that the binding of RNA (substrate and product) to TGT is much faster than the apparent $k_{formation}$ that we have measured from single-turnover, rapid quench studies. Therefore, it is reasonable to assign $k_{formation}$ as a lower limit for the chemical formation rate; any reverse reaction would mean that the chemical step would be faster than $k_{formation}$. While we were only able to estimate the observed breakdown rate for the slower phase for

$(dG)_{34}$ECYMH, given the pseudo-first order conditions, this value is a reasonable lower limit for the chemical breakdown step. From this, it is apparent that the dissociation of the product RNA is the overall rate-limiting step in the reaction.

It has previously been shown that the 2′-hydroxyl group of G34 is not requisite for the TGT reaction (11). Both the rates of formation and k_{cat} values for the RNA and 2′-deoxy RNA are essentially identical (Table 2). However, only the $(dG)_{34}$ECYMH covalent intermediate was isolated sufficiently to enable the measurement of the rate of breakdown. Presumably, the ECYMH covalent complex is significantly less stable (i.e., the equilibrium between the covalent complex and bound/free guanine and non-covalently bound RNA lies more toward the non-covalent complex). This is consistent with observations noted in the formation rapid-quench studies in which, for ECYMH, the maximum extent of covalent complex formed was about half that for $(dG)_{34}$ECYMH. This suggests that the rate of the back reaction for ECYMH (similar to breakdown but with guanine instead of $preQ_1$) is twice that for $(dG)_{34}$ECYMH. The 2′-hydroxyl group of G34 is located in a position to stabilize the incipient charge on aspartate 264 in the transition state for covalent complex breakdown (or reverse of formation), as schematically depicted in Figure 9. Additionally, a strong hydrogen bond could be formed between the 2′-hydroxyl group of G34 and the charged aspartate 264 in the ground state complex (perhaps mediated by a water molecule). In either event, the result would be stabilization of either the transition state or the ground state relative to that for $(dG)_{34}$ECYMH resulting in faster collapse of the intermediate for ECYMH.

In summary, these studies have unequivocally demonstrated that the TGT-RNA covalent complex is kinetically competent to be on the TGT reaction pathway. The evaluation of the rate constants for various chemical and binding steps has revealed that the dissociation of product RNA from the enzyme is overall rate-limiting in the steady-state. Further, studies comparing RNA with a 2′-deoxyriboside at the site of modification suggest a role for the 2′-hydroxyl group in stabilizing the growing negative charge on the nucleophilic aspartate (264) as the glycosidic bond to the aspartate is broken during covalent complex breakdown.

Supplementary Material

Refer to Web version on PubMed Central for supplementary material.

Acknowledgments

We would like to thank Prof. Carol Fierke and Dr. Katherine Bowers for assistance with the rapid quench experiments and Prof. Jason Gestwicki and Mr. Srikanth Patury for assistance with the BIAcore SPR studies and helpful discussions. We also wish to acknowledge the assistance of James Windak in the UM, Department of Chemistry, mass spectrometry facility.

The abbreviations used are

DTT	dithiothreitiol
ECYMH	hairpin RNA corresponding to the $tRNA^{tyr}$ anticodon stem-loop
HEPES	hydroxyethylpiperazine-ethylsulfonate
PAGE	polyacrylamide gel electrophoresis
PMSF	phenylmethylsulfonyl fluoride
Q	queuine
RRU	Relative Response Units

SDS	sodium dodecyl sulfate
SPR	Surface Plasmon Resonance
TCA	trichloroacetic acid
TGT	tRNA-guanine transglycosylase
Tris•HCl	tris(hydroxymethyl) aminomethane hydrochloride

References

1. Grosjean, H.; Benne, R. Modification and Editing of RNA: The Alteration of RNA Structure and Function. ASM Press; Washington, D. C: 1998.
2. Spedaliere CJ, et al. The pseudouridine synthases: Revisiting a mechanism that seemed settled. Journal of the American Chemical Society 2004;126:12758–12759. [PubMed: 15469254]
3. Romier C, et al. Mutagenesis and crystallographic studies of *Zymomonas mobilis* tRNA-guanine transglycosylase reveal aspartate 102 as the active site nucleophile. Biochemistry 1996;35:15734–15739. [PubMed: 8961936]
4. Zechel DL, Withers SG. Glycosidase mechanisms: Anatomy of a finely tuned catalyst. Accounts of Chemical Research 2000;33:11–18. [PubMed: 10639071]
5. Kittendorf JD, et al. tRNA-guanine transglycosylase from *Escherichia coli*: Molecular mechanism and role of aspartate 89. Biochemistry 2001;40:14123–14133. [PubMed: 11714265]
6. Kittendorf JD, et al. An essential role for aspartate 264 in catalysis by tRNA-guanine transglycosylase from *Escherichia coli*. Journal of Biological Chemistry 2003;278:42369–42376. [PubMed: 12909636]
7. Goodenough-Lashua DM, Garcia GA. tRNA-Guanine Transglycosylase from *Escherichia coli*: a Ping-Pong Kinetic Mechanism is Consistent with Nucleophilic Catalysis. Bioorganic Chemistry 2003;31:331–344. [PubMed: 12877882]
8. Chervin SM, Kittendorf JD, Garcia GA. Probing the Intermediacy of Covalent RNA-Enzyme Complexes in RNA Modification Enzymes. Methods in Enzymology 2007;425:121–137. [PubMed: 17673081]
9. Curnow AW, et al. tRNA-Guanine Transglycosylase from *Escherichia coli*: Gross tRNA Structural Requirements for Recognition. Biochemistry 1993;32:5239–5246. [PubMed: 8494901]
10. Nonekowski ST, Garcia GA. tRNA Recognition by the *E. coli* TGT: the Role of U33 in U-G-U Sequence Recognition. RNA 2001;7:1432–1441. [PubMed: 11680848]
11. Nonekowski ST, Kung FL, Garcia GA. The Escherichia coli tRNA-Guanine Transglycosylase Can Recognize and Modify DNA. Journal of Biological Chemistry 2002;277:7178–7182. [PubMed: 11751936]
12. Xie W, Liu XJ, Huang RH. Chemical trapping and crystal structure of a catalytic tRNA guanine transglycosylase covalent intermediate. Nature Structural Biology 2003;10:781–788.
13. Fersht, A. Structure and Mechanism In Protein Science: A Guide to Enzyme Catalysis and Protein Folding. W.H. Freeman and Company; New York: 1999.
14. Geeganage, s; Frey, PA. Transient Kinetics of Formation and Reaction of the Uridylyl-Enzyme Form of Galactose-1-P Uridylyltransferase and Its Q168R-Variant: Insight into the Molecular Basis of Galactosemia. Biochemsitry 1998;37:14500–14507.

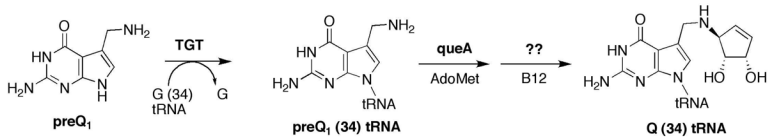

preQ$_1$ preQ$_1$ (34) tRNA Q (34) tRNA

Fig. 1.
Eubacterial tRNA-Guanine Transglycosylase (TGT) Pathway.

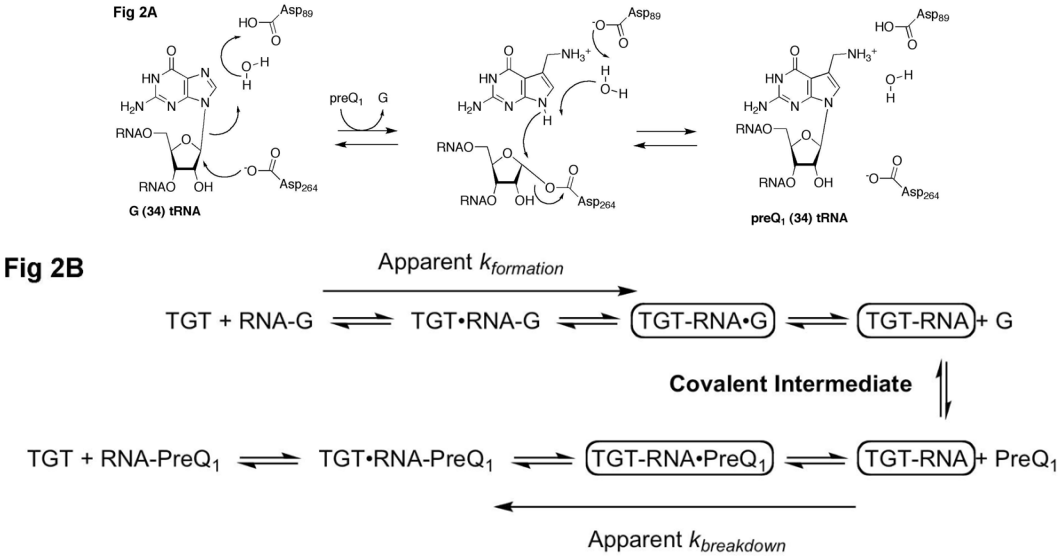

Fig. 2.

E. coli TGT Chemical and Kinetic Mechanisms. A: Chemical mechanism involving nucleophilic catalysis by aspartate 264. B: Ping-pong kinetic mechanism. Intermediates containing the covalent TGT-RNA complex are indicated.

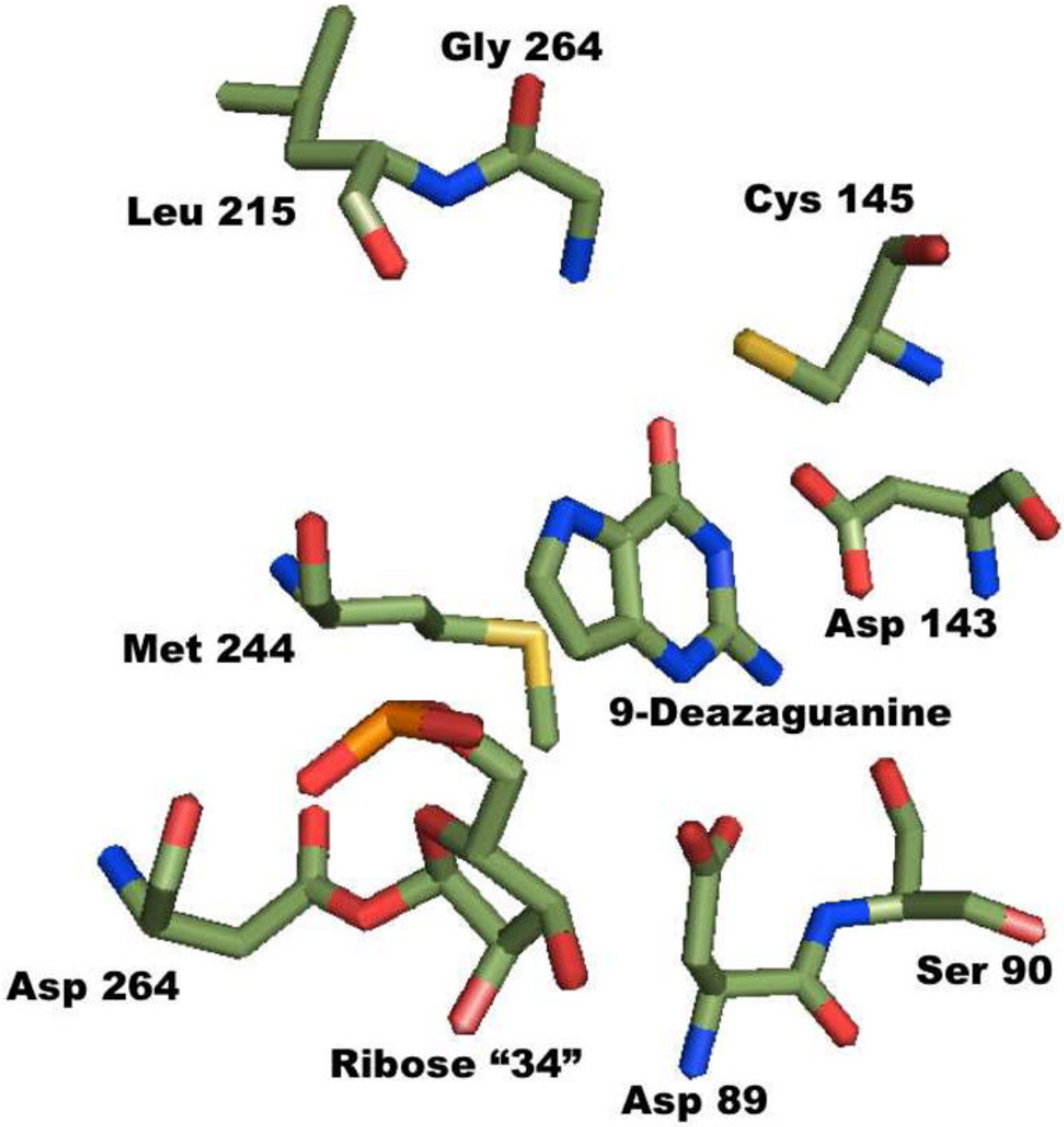

Fig. 3.
X-ray Crystal Structure of *Z. mobilis* TGT-RNA Covalent Complex Trapped with 9-Deazaguanine. Generated from PDB 1Q2R & 1Q2S, Xie, et al. (2003) *Nature Structural Biology* 10, 781–788.

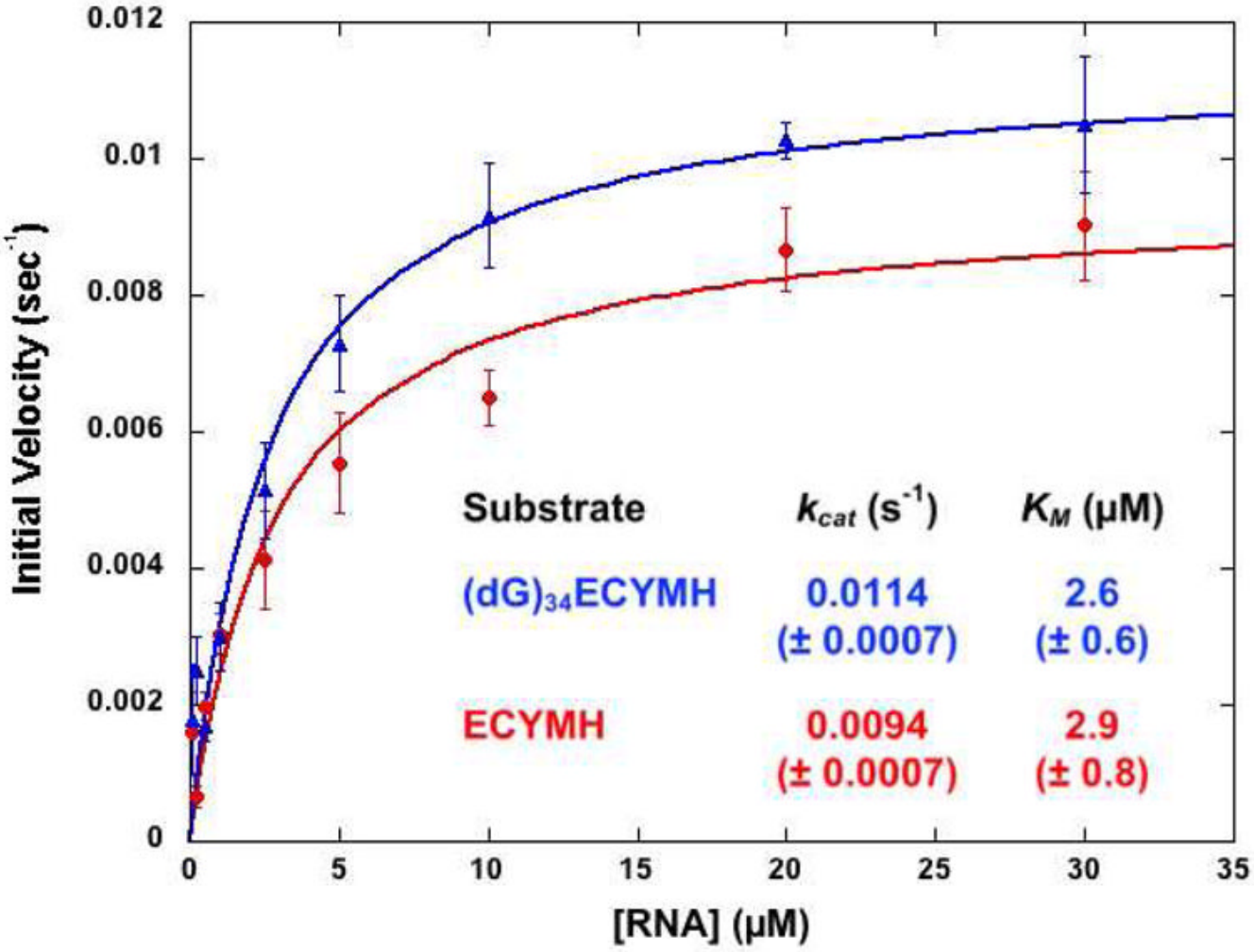

Fig. 4.

Steady-State Kinetics of $PreQ_1$ Incorporation for ECYMH and (dG_{34})ECYMH. Fits of initial velocity versus [RNA] to the Michaelis-Menten equation: $v_i = (k_{cat} \times [TGT])/(K_M + [RNA])$. Error bars are standard deviations of the averages of three independent trials. Kinetic parameters are reported with standard errors in parentheses.

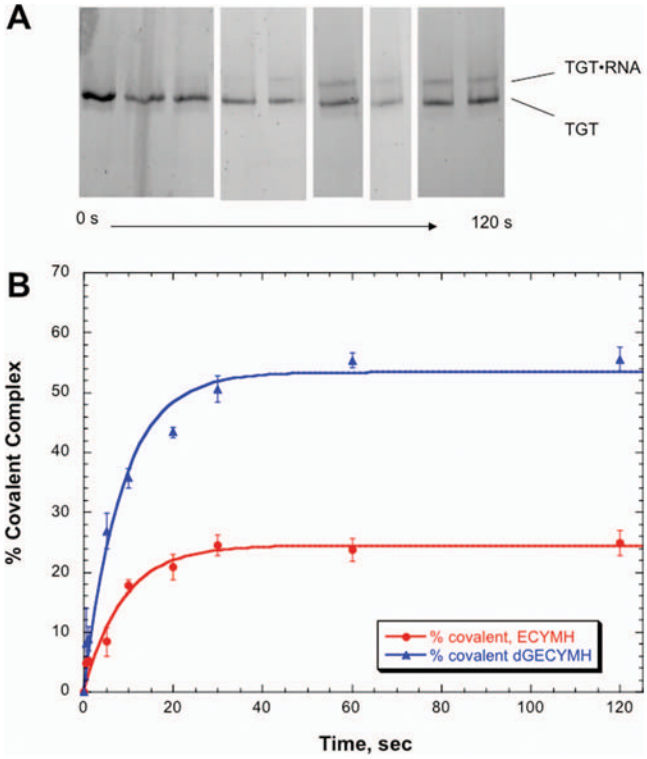

Fig. 5.

Kinetics of Covalent Complex Formation for ECYMH and (dG_{34})ECYMH. A: SDS-PAGE of TGT and TGT-ECYMH covalent complex versus time. Samples were obtained via rapid-quench as described in Experimental Procedures. B: Fit of % covalent versus time to an exponential binding equation: % covalent = A × (1 − exp(−$k_{formation}$ × time); where A = the maximum % covalent achieved. Error bars are ± standard deviation of time points from triplicate runs.

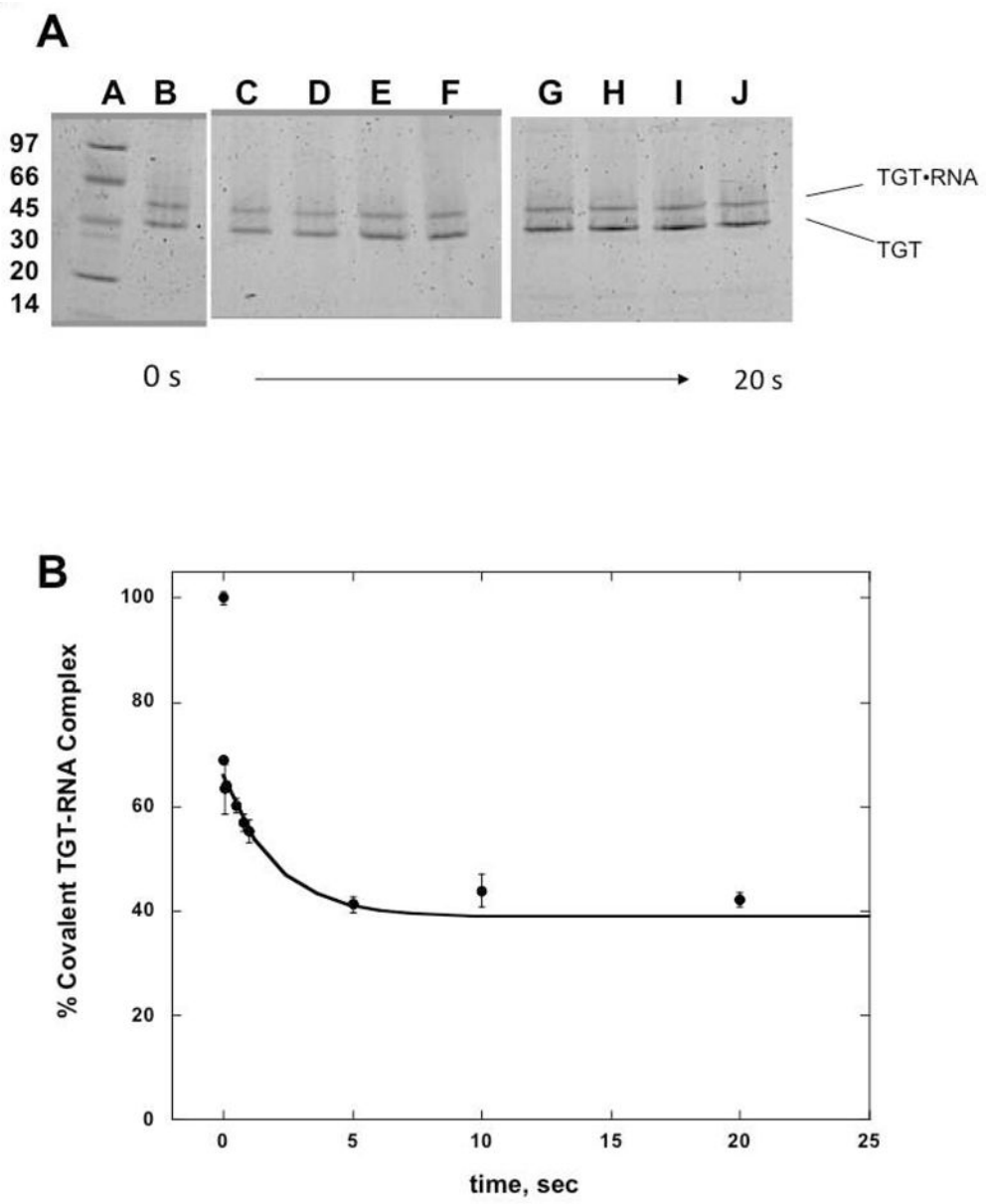

Fig. 6.

Kinetics of Covalent Complex Breakdown for (dG_{34})ECYMH. A: SDS-PAGE of TGT and TGT-RNA covalent complex versus time. Samples were obtained via rapid-quench as described in Experimental Procedures. B: Fit of % covalent versus time to a single exponential decay: % covalent = (A−B) × exp(−$k_{formation}$ × time) + B; where A = the initial % covalent (after the first rapid phase) and B = the limiting % covalent. Note that the first data point was omitted from the fit. See Results for discussion. Error bars are ± standard deviation of time points from four runs.

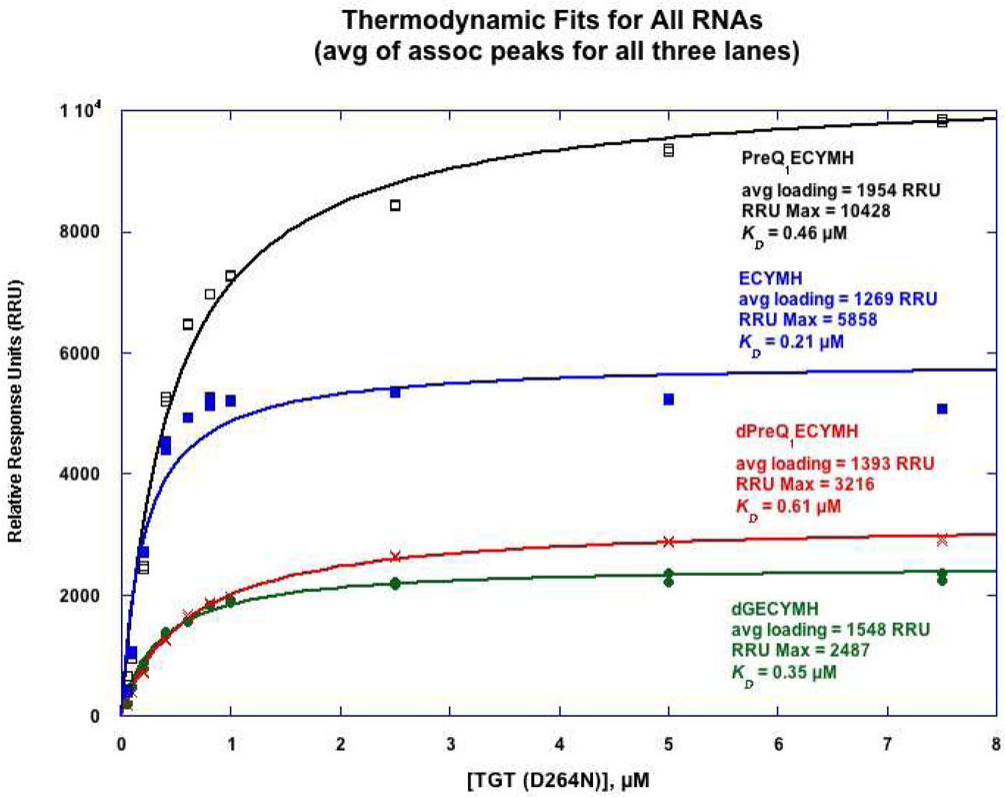

Fig. 7.

Thermodynamic Fit of SPR Association Peak Values to Determine K_D^*s. Association peak RU values of replicate runs for each RNA were fit to the steady-state binding equation: $RU_{obs} = (RU_{max} \times [TGT(D264N)])/(K_D + [TGT(D264N)])$. The average RNA loadings for each chip are indicated.

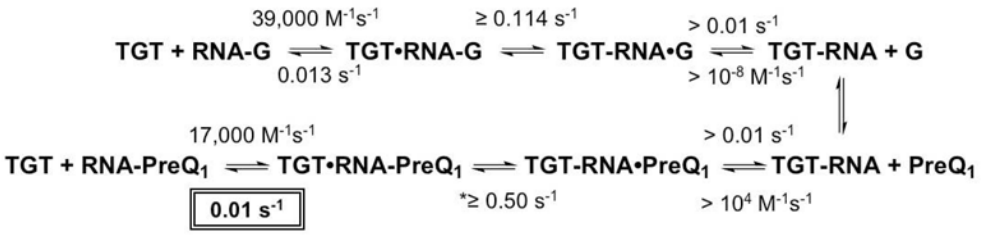

Fig. 8.

E. coli TGT Kinetic Mechanism with Rate Constant Values. The rate constant for the chemical step of formation of the covalent intermediate is a lower limit estimated from $k_{formation}$. The rate constant for the breakdown of the covalent intermediate (*0.50 s^{-1}) is an estimate of the slower phase. Lower limits for the on- and off-rates for guanine and $preQ_1$ can be made by setting the lower limit for the forward steps (off-rate for guanine and on-rate for $preQ_1$) ≥ 0.01 s^{-1} (k_{cat}). Assuming K_M approximates K_D, then lower limits for the other rates can be set by simple division ($K_D = k_{off}/k_{on}$). The overall rate-determining step is the dissociation of product tRNA (boxed).

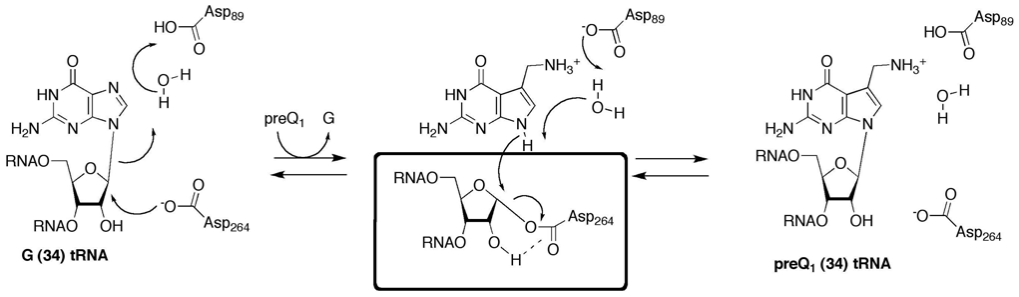

Fig. 9.
Proposed Role of 2′-Hydroxyl group in Breakdown of TGT-RNA Covalent Complex.

Table 1

Apparent Rates of Formation and Breakdown of Covalent Intermediate

RNA	*Apparent* $k_{formation}$ (s^{-1})	*Apparent* $k_{breakdown}$ (s^{-1})	k_{cat} (s^{-1})
ECYMH	**0.114** ± 0.021	**nd**	**0.0094** ± 0.0007
(dG_{34})ECYMH	**0.118** ± 0.017	**0.50** ± 0.14	**0.011** ± 0.0007

(Rates are reported ± standard error of the fits; nd = not determined)

Table 2

Binding and Steady-State Kinetic Parameters

RNA	k_{on} (M^{-1} s^{-1})	k_{off} (s^{-1})	K_D (μM) (k_{off}/k_{on})	K_D^* (μM)	k_{cat} (s^{-1})	K_M (μM)
ECYMH	**39,000**± 1000	**0.013**± 0.001	**0.33**± 0.11	**0.21**± 0.04	**0.0094**± 0.0007	**2.87**± 0.77
($PreQ_1$) ECYMH	**17,000**± 9600	**0.010**± 0.005	**0.66**± 0.33	**0.46**± 0.05	**na**	**na**
(dG_{34}) ECYMH	**84,000**± 28,000	**0.026**± 0.001	**0.31**± 0.11	**0.35**± 0.02	**0.011**± 0.0007	**2.62**± 0.62
($dPreQ_1$) ECYMH	**74,000**± 22,000	**0.021**± 0.005	**0.28**± 0.16	**0.61**± 0.02	**na**	**na**

On and off rate constants were determined from a fit to a two-state model (below). Only the values for the on and off rate constants were used to calculate K_Ds. The full set of values can be found in Supplementary Material. K_D^* was determined from a "thermodynamic fit" of association peak values (Figure 10). K_M and k_{cat} values were determined from Michaelis-Menten fits (Figure 7). Parameters are reported ± standard error of the fits. na = not applicable as (preQ1)ECYMH is not a substrate.